PHYSICAL REVIEW B **81**, 241407(R) (2010)

Capillary force induced structural deformation in liquid infiltrated elastic circular tubes

Y. Yang,[1] Y. F. Gao,[1] D. Y. Sun,[1] M. Asta,[2,3] and J. J. Hoyt[4]
[1]*Department of Physics, East China Normal University, Shanghai 200062, People's Republic of China*
[2]*Department of Materials Science and Engineering, University of California, Berkeley, California 94720, USA*
[3]*Department of Chemical Engineering and Materials Science, University of California, Davis, California 95616, USA*
[4]*Department of Materials Science and Engineering, McMaster University, Hamilton, Ontario, Canada*
(Received 22 January 2010; published 9 June 2010)

The capillary-induced structural deformation of an elastic circular tube partially filled by a liquid is studied by combining theoretical analysis and molecular-dynamics simulations. The analysis shows that, associated with the deformation, there is a well-defined length scale (elastocapillary length), which exhibits a scaling relationship with the characteristic length of the tube, regardless of the interaction details. We validate this scaling relationship for a carbon nanotube partially filled by liquid iron. The capillary-induced structural transformation could have potential applications for nanodevices.

DOI: 10.1103/PhysRevB.81.241407 PACS number(s): 68.08.De, 46.32.+x, 61.48.De

A wide range of phenomena in nature, which span from everyday observations to many bio-related processes, are a result of capillary forces. Common examples include the shape of liquid droplets, the imbibition of a sponge,[1] the clumping of wet hair into bundles[2] and coalescence of paintbrush fibers,[3] the standing of aquatic insects on water,[4] lung airway closure, etc.[5] Recently it was found that capillary forces can induce structural deformations or instability in an elastic system, in cases where these surface forces are comparable in magnitude to bulk elastic forces. More importantly, there is a well-defined length scale (elastocapillary length L_{EC}) which underlies such structural instabilities,[6] which usually reveals an intrinsic scaling relation with the characteristic dimensions.[2,3,6–9] The elastocapillarity deformation or instability has been also found to have many interesting applications.[7,8,10,11]

Liquid infiltrated elastic tubes are common in biosystems and everyday life. When the capillary forces are comparable to the bending stiffness of the tube, the tube can be deformed or become unstable at some critical filling fraction. Whether the deformation can be associated with a new type of scaling relationship has thus far remained relatively unexplored. In this work, molecular-dynamics (MD) simulations of this phenomenon are coupled with theoretical analysis to investigate this issue for an elastic cylindrical tube partially filled by a liquid. Our results show that the deformation of a flexible tube leads to a well-defined scaling law regardless of the interaction details. Our MD simulations on liquid iron encapsulated by carbon nanotubes (CNTs) quantitatively demonstrate the scaling law.

We consider an elastic circular tube with length of L_t and radius of R_0 partially filled with an incompressible Newtonian liquid of length L_l, where R_0 refers the radius of the "dry" tube without any compression. The upper panel of Fig. 1 illustrates the model used in the current work. The energy of the system can be written formally as

$$E = E_b + E_c + E_i, \tag{1}$$

where E_b, E_c, and E_i are the elastic bending strain energy, elastic compression strain energy, and interfacial free energy (capillary energy), respectively. In the continuum elasticity picture,[12,13] the bending strain energy is $E_b = \frac{L_t B}{2}\oint \frac{1}{\rho^2} dl$, and the compression strain energy is $E_c = \frac{L_t C}{2}\oint (\frac{\oint dl - P_0}{P_0})^2 dl$, where $\oint$ denotes the curvilinear integral along the perimeter of the cross section and $P_0 = 2\pi R_0$ is the perimeter of the original tube cross section. The bending stiffness $B = Yh^3/12(1-\nu^2)$ and the compression stiffness $C = Yh/(1-\nu^2)$ are constants related to Young's modulus Y, the Poisson ratio ν, and the tube thickness h. The local radius of curvature is denoted as ρ. In current studies, the tubes with small h are considered, thus the compression stiffness is much stronger than the bending stiffness. Under this condition, the length change in the axial direction is neglected. The interfacial free energy is $E_i = A_{lv}\gamma_{lv} + A_{sl}\gamma_{sl} + A_{sv}\gamma_{sv} + 2P\tau$, where A_{lv}, A_{sl}, and A_{sv} are the areas of liquid-vapor, solid-liquid, and solid-vapor inter-

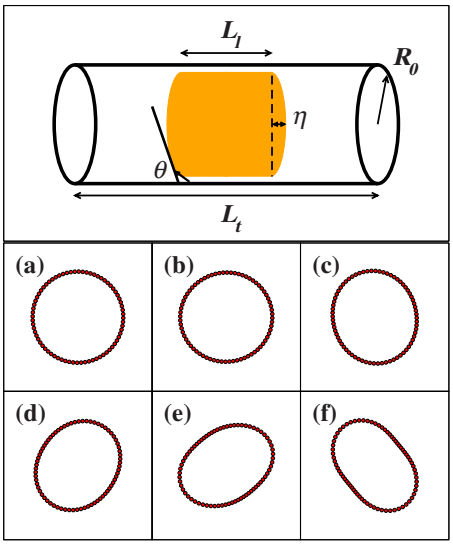

FIG. 1. (Color online) Upper panel: sketch of the model used in present work. The elastic tube is characterized by length (L_t) and radius (R_0). The encapsulated liquid is described by the length (L_l), the height of cap (η), and the contact angle (θ). Lower panel: time-averaged cross section for various lengths of the CNT L_t. All results are for (40,0) CNTs with liquid length L_l=16.85 Å. (a) L_t =96.92 Å, (b) L_t=84.28 Å, (c) L_t=59.00 Å, (d) L_t=50.58 Å, (e) L_t=46.36 Å, and (f) L_t=42.15 Å.

faces, respectively, P is the perimeter of the cross section and $A_{sv}=2PL_t-A_{sl}$. Here we have included the solid-vapor surface outside the cylinder that is not covered by liquid. The surface and interface free energies are denoted γ_{lv}, γ_{sl}, and γ_{sv}, for the liquid-vapor, solid-liquid, and solid-vapor interfaces, respectively. The specific free energy of the three-phase contact line (i.e., the line tension) is denoted as τ.[14] The $2P\tau$ term usually can be neglected if the dimension of the system is not too small.

Since only near-critical sizes (where the circular shape is near its stability limit) are considered, the noncircular shape is approximated by that of an ellipse. The reasons for assuming an oval shape are twofold: (1) our numerical tests suggest the oval shape; (2) oval shapes were obtained in previous studies of tubes under uniform radial pressure.[15] It should be pointed out that the shape of the tube cross section can be much more complicated under large deformations.[16] For an ellipse with long axis R_a and short axis R_b, the shape can be described well by introducing two independent variables, R and ω, which are defined as $R=\sqrt{R_aR_b}$ and $\omega=R_a/R_b$. When $\omega=1$, these variables describe a perfect circle. By introducing two integrals, $f_{1,2}(\omega)=\frac{1}{2\pi}\oint(\omega\cos^2 t+\omega^{-1}\sin^2 t)^{\alpha_{1,2}}dt$, with $\alpha_1=-2.5$ and $\alpha_2=0.5$, we can write $\oint\frac{1}{\rho^2}dl=\frac{2\pi}{R}f_1(\omega)$ and $\oint dl=P=2\pi Rf_2(\omega)$.[15] Finally, we have

$$E_b+E_c=\frac{B\pi L_t}{R}f_1(\omega)+C\pi R_0L_t\left\{\left[\frac{R}{R_0}f_2(\omega)\right]^3-2\left[\frac{R}{R_0}f_2(\omega)\right]^2+\frac{R}{R_0}f_2(\omega)\right\}. \quad (2)$$

In order to calculate the capillary energy, the area of the interfaces should be written in explicit forms. However, the general calculation of the liquid-vapor interface, which is a meniscus, for arbitrary tube shape is beyond the scope of the present treatment and will be discussed in a subsequent paper.[17] To elucidate the important physics as well as to simplify the mathematical treatment, we consider the cases where the contact angles are close to 90°. Within this limitation, all the interface areas can be defined without ambiguity. It should be noted that in the simulations discussed below, the solid-liquid contact angles are in fact approximately 90°.

The deformations that break symmetry along the axis and thermal fluctuations of the tubes are neglected as they exist on a length scale comparable to the persistence length ($l_p=YI/k_BT$, and Y: Young's modulus, I: the area moment of intertia.), which usually is much longer than the characteristic length of system. For example, in single-walled carbon nanotubes (SWCNTs), the persistence length is on the order of 45 μm.[6] With the above assumptions as well as the assumption of that the liquid is incompressible, we can write $A_{lv}=2\pi R^2$, $A_{sl}=PL_l(\frac{R_0^2}{R^2})$, and $A_{sv}=2PL_t-A_{sl}$. So, the interfacial free energy is

$$E_i=2\pi R^2\gamma_{lv}+PL_l\frac{R_0^2}{R^2}(\gamma_{sl}-\gamma_{sv})+2PL_t\gamma_{sv}+2P\tau. \quad (3)$$

In Eq. (2), the elastic energy always tends to maintain the tube in a circular shape. If the capillary energy approaches or exceeds the magnitude of the elastic energy, the circular shape will be unstable and the system might seek a lower-energy state. Physically, the deformation of the tube reduces the interfacial energy at the cost of increasing the elastic energy. For $\theta<90°$, $(\gamma_{sl}-\gamma_{sv})<0$, the system could deform to increase the area of the solid-liquid interface. Even for $\theta\geq 90°$, $(\gamma_{sl}-\gamma_{sv})\geq 0$, the tube still has a chance to deform if the first term exceeds the second term in Eq. (3), in which case the area of the liquid-vapor interface decreases. The MD simulations in the current work focus on the latter case. The critical transition point can be located by the condition $\frac{\partial^2 E}{\partial\omega^2}|_{\omega=1}=0$ and the radius of tube at the critical point (R_c) is determined by $\frac{\partial E}{\partial R}|_{\omega=1}=0$. Remembering $f_{1,2}(\omega)|_{\omega=1}=1$, $f'_{1,2}(\omega)|_{\omega=1}=0$, and $f''_{1,2}(\omega)|_{\omega=1}=\frac{15}{8},\frac{3}{8}$, the above conditions produce the critical relation,

$$L_t^*=\frac{2\left[\gamma_{lv}-(\gamma_{sl}-\gamma_{sv})\frac{L_lR_0^2}{R_c^3}\right]R_c^3}{3B}, \quad (4)$$

where L_t^* is the critical length of the tube. For elastic tubes, if the compression stiffness (C) is much larger than the bending stiffness B, which is the case we are interested in, one can neglect the difference between R_0 and R_c,

$$L_t^*=\frac{2\left[\gamma_{lv}-(\gamma_{sl}-\gamma_{sv})\frac{L_l}{R_0}\right]R_0^3}{3B}. \quad (5)$$

We can define an effective interface free energy $\gamma^*=[\gamma_{lv}-(\gamma_{sl}-\gamma_{sv})\frac{L_l}{R_0}]$, where the factor $\frac{L_l}{R_0}$ in γ^* reflects an inherent geometric relation among the three interfaces. Note that if $2\gamma^*$ is divided L_t^*, according to Eq. (5), a generalized pressure $p^*=\frac{2\gamma^*}{L_t^*}=\frac{3B}{R_0^3}$ can be obtained, which is the same form as reported in Ref. 15 for CNTs under pressure. In fact, this capillary force can be regarded as a kind of negative internal pressure. From Eq. (5), a generalized elastocapillary scaling relation can be derived,

$$\left[\frac{2R_0^3}{3L_t^*}\right]^{1/2}=\left[\frac{B}{\gamma^*}\right]^{1/2}. \quad (6)$$

Similar to previous studies,[2,3,6–9] we can define an elastocapillary length ($L_{EC}=[\frac{B}{\gamma^*}]^{1/2}$) for this system, which gives the typical effective curvature induced by capillarity on the tube. Different from previous studies, the elastocapillary length is not simply defined in terms of interfacial free energies but rather an effective (average) interface free energy (γ^*). The difference stems from the fact that in the filled liquid tube system studied here, the area of the solid-liquid (solid-vapor) and liquid-vapor interfaces changes in different ways (amounts) as the tube is deformed. The former scales as R while the later scales as R^2. It implies that the average capillary forces depend on the system size itself ($\frac{L_l}{R_0}$ in γ^* reflects the dependence). However, in previous studies, either the three interfaces change simultaneously by the same amount (liquid drop on thin films)[7,8] or only one interface changes area (e.g., slender rods immersed in liquid),[2,3,6,9] and thus the average capillary force is independent of the size of system.

We can also define a characteristic length of the system at the critical point, $L_C = \frac{Area\ of\ cross\ section}{Surface\ area\ of\ tube} = \frac{2\pi R_0^2}{\sqrt{2\pi R_0 L_t^*}} = \sqrt{3\pi}(\frac{2R_0^3}{3L_t^*})^{1/2}$, which is a purely geometric description of the tube. Equation (6) becomes a generic scaling relationship,

$$L_C = \sqrt{3\pi} L_{EC}. \tag{7}$$

L_C defines a typical length scale at which the elastic energy and surface energy are comparable. Different from previous studies for slender rods immersed in liquid,[2,3,6,9] or for liquid drops on thin films,[7,8] the characteristic length in the present case is not simply a spatial dimension of the system. The reason is that the elastic energy depends on both R_0 and L_t, where R_0 and L_t are functions of the radial bulk modulus and total elastic energy, respectively. Therefore, the elastocapillary length and the scaling relationship presented here represent a new type of deformation process.

To test the theoretical analysis, we simulate liquid iron encapsulated by a SWCNT using MD simulation. We want to point out that the MD simulation is not meant to suggest a specific system for realistic application but rather to test the validity of the mathematical model. All the simulations made use of the LAMMPS (large-scale atomic/molecular massively parallel simulator) code.[18] The interaction between carbon atoms is described by the second-generation reactive empirical bond order (REBO2) potential.[19] The many-body potential developed by Mendelev *et al.* is used to describe the Fe-Fe interactions.[20] The weak interaction between C and Fe is modeled by a truncated Lennard-Jones potential.[21,22] The interaction parameters σ and ϵ are obtained by fitting to *ab initio* results,[23] σ=2.05 Å and ϵ=0.09463 eV. The *ab initio* results are also used by other authors to fit the C-Fe interaction based on Johnson pair form potential.[24] This fitted potential gives a reasonable contact angle (~107° at 2500 K) compared to the experimental value (~125° at 923 K) for liquid Fe in SWCNT.[25]

In the present study, periodic boundary conditions in the axial direction and free boundary conditions in the radial directions are adopted. To test the effect of the axial stress on the final results, we have made both constant tube length and constant axial stress simulations, no noticeable difference was observed in our studies. All the MD results presented here are obtained based on the zero axial stress boundary condition by using a constant-pressure MD scheme. The systems are simulated at T=2500 K and zero pressure. The temperature is much higher than the melting point of Fe (Ref. 20) so that Fe is in a well-defined liquid state. A typical run lasts 3 ns for each case. The tubes used in this work are of the zigzag type, with tube indices (32,0), (40,0), (46,0), and (50,0), and the typical length in the range of 30–250 Å. To locate the critical length for each sample, the length of the tube is decreased until the circular shape of the CNT becomes unstable.

To quantitatively compare the model prediction and MD results, the value of all the variables on the right-hand side of Eq. (5) are needed. γ_{lv} for liquid iron at 2500 K is calculated separately using the method reported in Refs. 26 and 27, the value obtained is about 0.82 ± 0.02 J/m^2. Both $(\gamma_{sl} - \gamma_{sv})$ and τ can be calculated from the extended Young's equation[14] if the contact angle as a function of the radius of the CNT is known. Contact angles θ are measured during MD simulations for a circular shape. The determination of the contact angle follows the procedure described in Refs. 28 and 29. We obtain $\gamma_{sl} - \gamma_{sv} = 0.24 \pm 0.02$ J/m^2 and $\tau = 0.4 \times 10^{-10} \pm 0.3 \times 10^{-10}$ J/m. The elastic constant B of the CNT for the REBO2 potential is adopted from Ref. 30, B = 1.4 eV.

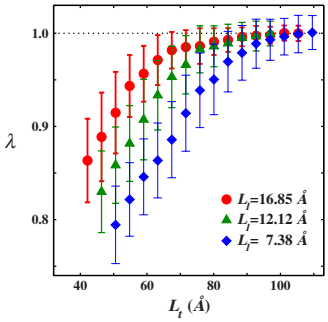

FIG. 2. (Color online) The order parameter λ versus the length of the CNT (40,0). Circle: length of liquid L_l=16.85 Å, triangle: length of liquid L_l=12.12 Å, and diamond: length of liquid L_l =7.38 Å.

The measurement of the CNT shape is based on the calculation of the cross-sectional area S. An order parameter thus can be defined as $\lambda = \langle S \rangle_t / S_0$, where S_0 is the initial cross-sectional area of the CNT and $\langle \cdots \rangle_t$ denotes the time average. With this definition λ is one for the circular shape while it is smaller than one for a noncircular shape, and decreases continuously with increasing deviation from a circular shape. Due to thermal fluctuations, the shape of the CNT varies with time. We define the critical length for which λ is smaller than one within the statistical uncertainty.

The lower panel of Fig. 1 shows the time-averaged cross section for a (40,0) CNT filled with 16.85 Å liquid for a few selected L_t. With decreasing L_t, the shape of the cross section changes from a circle to an ellipse. Figure 2 shows the evolution of λ vs the length of the CNT (L_t) for a (40,0) tube, where the different symbols denote systems with different lengths of liquid. We find that the order parameter can clearly distinguish the CNT shape change from circle to ellipse. From Fig. 2, one can see that, for longer L_t, λ remains at an average value of one (corresponding to a circular shape) within the error bars while λ deviates from one for shorter L_t. The critical length can be located from this figure. It should be pointed out that the critical length is not dependent on the specific definition of order parameter. Another order parameter based on the Fourier spectrum of a shape fluctuation function[31,32] was also tested and the results do not show significant differences. For all studied samples, when L_t is smaller than a certain critical length, the shape of the cross section will change from circle to ellipse. The shape changes are purely elastic deformations and the system can relax reversibly by removing the liquid.

Figure 3 shows the critical length of the tube L_t^* vs the liquid length L_l for all CNTs studied, where the solid line is plotted based on Eq. (5) using the parameter values given above. One can see that the MD results are in excellent

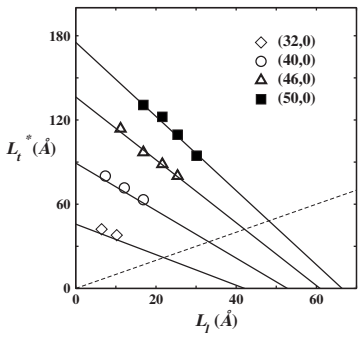

FIG. 3. The critical length of the tube as a function of the length of liquid filled region. Symbols: the molecular-dynamics results, solid lines: the analysis results of Eq. (5), dashed lines: the tube is fully filled with liquid, below this line the model is not valid.

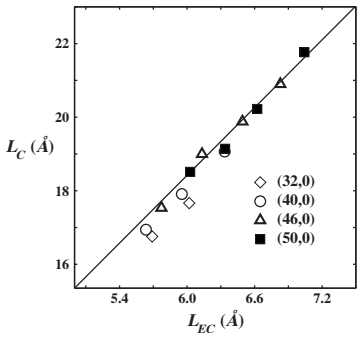

FIG. 4. The characteristic geometry length as a function of elastocapillary length. Symbols: the molecular-dynamics results, lines: analysis results of Eq. (7).

agreement with the theoretical predictions. The MD results are consistent with a linear relationship between L_C and L_{EC} as expected from the model analysis (see Fig. 4). A best fit produces a slope of 3.034 ± 0.014, which is in excellent agreement with the theoretical prediction of $\sqrt{3\pi}$.

The critical length [Eq. (5)] affords a few potential applications in nanoscience or in designing nanodevices. One possible application is the measurement of the elastic bending stiffness (B) of the tube or the contact angle. For this purpose, we only need knowledge of L_l^* as a function of L_l by filling liquid into the tubes. If the γ_{lv} and contact angle are known, B can be obtained. On the other hand, if B is known, the contact angle can be estimated. The capillary-induced structural transformation also provides an ideal mechanism of conversion of capillary energy to elastic energy. If the values of the interface energies in Eq. (5) are sensitive to the temperature or to other environment variables, an environment-controlled nanomachine could be achieved. Experimentally, hollow polymer tubes (PTs) with specific diameter and wall thickness are routinely synthesized.[33] Usually, PTs are much softer than CNTs, and so these materials are ideal candidates for observing the phenomena described in this work.

In summary, the capillary-induced deformation of elastic circular tubes has been studied by combining theoretical analysis and MD simulation. The deformation depends on two key length scales, the elastocapillary length L_{EC} which represents the typical radius of curvature produced by capillary forces on an elastic tube and the characteristic geometric length L_C, which defines a typical reduced size of the tube. At the critical point, L_C is found to be proportional to L_{EC}, above which a tube preserves a circular shape. The MD results are found to be in excellent agreement with the theoretical prediction. The current results can be useful to the design of nanodevices.

We thank B. B. Laird for his helpful discussion. This work is supported by the National Natural Science Foundation of China, Shanghai Project for the Basic Research. The computation is performed in the Supercomputer Center of Shanghai and the Supercomputer Center of ECNU.

[1] P.-G. de Gennes *et al.*, *Capillarity and Wetting Phenomena: Drops, Bubbles, Pearls, Waves* (Springer, New York, 2003).
[2] J. Bico *et al.*, Nature (London) **432**, 690 (2004).
[3] H.-Y. Kim *et al.*, J. Fluid Mech. **548**, 141 (2006).
[4] D. L. Hu *et al.*, Nature (London) **437**, 733 (2005).
[5] M. Heil *et al.*, Respir. Physiol. Neurobiol. **163**, 214 (2008).
[6] A. E. Cohen *et al.*, Proc. Natl. Acad. Sci. U.S.A. **100**, 12141 (2003).
[7] C. Py *et al.*, Phys. Rev. Lett. **98**, 156103 (2007).
[8] J. Huang *et al.*, Science **317**, 650 (2007).
[9] S. Neukirch *et al.*, J. Mech. Phys. Solids **55**, 1212 (2007).
[10] N. Chakrapani *et al.*, Proc. Natl. Acad. Sci. U.S.A. **101**, 4009 (2004).
[11] B. Pokroy *et al.*, Science **323**, 237 (2009).
[12] L. D. Landau *et al.*, *Elasticity Theory* (Pergamon, Oxford, 1996).
[13] S. Timoshenko *et al.*, *Theory of Elastic Stability* (McGraw-Hill, New York, 1988).
[14] L. Boruvka *et al.*, J. Chem. Phys. **66**, 5464 (1977).
[15] D. Y. Sun *et al.*, Phys. Rev. B **70**, 165417 (2004).
[16] L. Boué *et al.*, Phys. Rev. Lett. **97**, 166104 (2006).
[17] Y. Yang *et al.* (unpublished).
[18] S. J. Plimpton, J. Comput. Phys. **117**, 1 (1995).
[19] D. W. Brenner *et al.*, J. Phys.: Condens. Matter **14**, 783 (2002).
[20] M. I. Mendelev *et al.*, Philos. Mag. **83**, 3977 (2003).
[21] J. Broughton *et al.*, Acta Metall. **31**, 845 (1983).
[22] R. L. Davidchack *et al.*, J. Chem. Phys. **118**, 7651 (2003).
[23] E. Durgun *et al.*, Phys. Rev. B **67**, 201401(R) (2003).
[24] F. Ding *et al.*, J. Phys. Chem. B **108**, 17369 (2004).
[25] D. C. Wei *et al.*, Adv. Mater. **19**, 386 (2007).
[26] M. J. P. Nijmeijer *et al.*, J. Chem. Phys. **89**, 3789 (1988).
[27] S. W. Sides *et al.*, Phys. Rev. E **60**, 6708 (1999).
[28] A. Kutana *et al.*, Phys. Rev. B **76**, 195444 (2007).
[29] T. Werder *et al.*, J. Phys. Chem. B **107**, 1345 (2003).
[30] Q. Lu *et al.*, J. Phys. D **42**, 102002 (2009).
[31] S. V. Khare *et al.*, Phys. Rev. B **54**, 11752 (1996).
[32] D. C. Schlößer *et al.*, Phys. Rev. Lett. **82**, 3843 (1999).
[33] R. Mueller *et al.*, J. Phys. Chem. B **111**, 8547 (2007).